JACS
JOURNAL OF THE AMERICAN CHEMICAL SOCIETY

Communication

pubs.acs.org/JACS

Photocatalytic Water Oxidation: Tuning Light-Induced Electron Transfer by Molecular Co_4O_4 Cores

Serena Berardi,[†] Giuseppina La Ganga,[‡] Mirco Natali,[§] Irene Bazzan,[†] Fausto Puntoriero,[‡] Andrea Sartorel,*[,†] Franco Scandola,*[,§] Sebastiano Campagna,*[,‡] and Marcella Bonchio*[,†]

[†]ITM-CNR and Department of Chemical Sciences, University of Padova, via F. Marzolo 1, 35131 Padova, Italy

[‡]Dipartimento di Chimica Inorganica, Chimica Analitica e Chimica Fisica, Università di Messina, and Centro Interuniversitario per la Conversione Chimica dell'Energia Solare (sez. Messina), via Sperone 31, 98166 Messina, Italy

[§]Chemistry Department, University of Ferrara, and Centro Interuniversitario per la Conversione Chimica dell'Energia Solare (sez. Ferrara), via L. Borsari 46, 44121 Ferrara, Italy

Supporting Information

ABSTRACT: Isostructural cubane-shaped catalysts $[Co^{III}_4(\mu\text{-}O)_4(\mu\text{-}CH_3COO)_4(p\text{-}NC_5H_4X)_4]$, **1-X** (X = H, Me, *t*-Bu, OMe, Br, COOMe, CN), enable water oxidation under dark and illuminated conditions, where the primary step of photoinduced electron transfer obeys to Hammett linear free energy relationship behavior. Ligand design and catalyst optimization are instrumental for sustained O_2 productivity with quantum efficiency up to 80% at $\lambda > 400$ nm, thus opening a new perspective for in vitro molecular photosynthesis

Aerobic life on Earth relies on a perpetual series of light-activated redox events, involving multiple and sequential photoinduced transfer of electrons and protons. Oxygenic photosynthesis is one prominent example, mastering the photo-oxidation of water as electron and proton source to build energy-rich carbohydrates to be used as food and thus providing a vital solar fuel.[1−3] With a similar perspective, light-activated water oxidation is also the crucial step of artificial photosynthesis.[4,5] This is the off-leaf transposition of the natural machinery, finalized to the continuous production of hydrogen, as renewable and carbon-neutral energy vector. The challenge herein is a generally low quantum efficiency (QE), which is mainly dictated by the high energy cost of the water oxidation step, by far the uphill bottleneck of the overall process. Lowering of this barrier with a bioinspired strategy can be accomplished by a tailored design of metal-based multi-electron catalysts.[5] These latter can foster the photoinduced removal of electrons and protons from metal-aquo inter-mediates via low-energy pathways, eventually powered by visible light.[5] State-of-the-art water oxidation catalysts (WOCs) are generally based on metal oxide colloids[6−11] or bulk surfaces,[12,13] and only a few examples have been actually reported and proved where discrete molecular complexes can activate photocatalytic cycles.[14−19] Molecular WOCs have a formidable appeal by virtue of a tunable set of ligands affecting the redox and kinetic properties of all photogenerated intermediates and reactive transients. One promising case stems from the interplay of carboxylate and pyridine ligands that can stabilize a tetracobalt core, with a cubane arrange-ment[20] and WOC properties.[21] The resulting complex, with formula $[Co^{III}_4(\mu\text{-}O)_4(\mu\text{-}CH_3COO)_4(NC_5H_5)_4]$ (**1-H**), de-serves particular attention since (i) cobalt is a low-cost and abundant metal, (ii) its tetranuclear oxo core mimics the natural oxygen-evolving complex of Photosystem II,[20,21] and (iii) it stands as the homogeneous analogue of the amorphous cobalt oxide/hydroxide film (Nocera's catalyst),[12] whose electro-catalytic potential has been recently exploited within light-activated devices.[22−24]

Indeed, molecular **1-H** can leverage water photooxidation cycles by the combined presence of the photosensitizer $Ru(bpy)_3^{2+}$ (bpy = 2,2′-bipyridine) and persulfate anion, $S_2O_8^{2-}$, as the sacrificial electron acceptor (Scheme 1a; for a complete reaction scheme, see Supporting Information). The resulting system, in water at pH 8, can reach a QE of 60% in

Scheme 1. (a) Light-Driven Water Oxidation with the $Ru(bpy)_3^{2+}/S_2O_8^{2-}$ System Catalyzed by 1-H and (b) Structural Representation of 1-X (X = Me, *t*-Bu, OMe, Br, COOMe, CN)

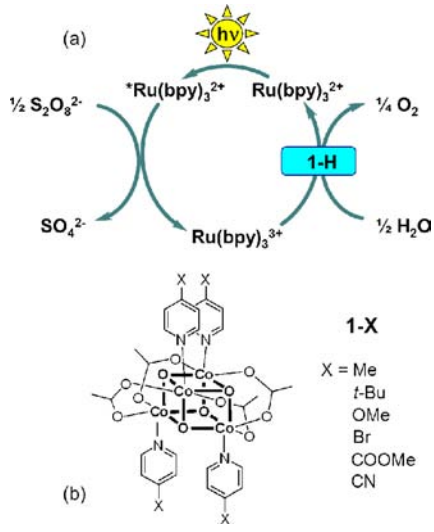

Received: April 24, 2012
Published: June 20, 2012

   dx.doi.org/10.1021/ja303951z | J. Am. Chem. Soc. 2012, 134, 11104−11107

terms of O_2 photoconversion,[21a,25] but the reaction kinetics and the overall productivity level off at ca. 30% of the sacrificial persulfate consumption.[21] While the catalyst photostability has been ascertained by ^{1}H NMR under turnover conditions,[21b] the weakness herein is the irreversible decomposition of the ruthenium sensitizer, switching off the process before completion and preventing long-term operation and/or recharge protocols.[21]

Our study targets ligand modification and catalyst optimization to boost photoinduced electron transfer (ET), photosynthetic yields, and QEs up to the outstanding value of 80%, while providing key descriptors of fundamental mechanistic aspects. Our approach focuses on diverse *para*-substituted pyridines selected as terminal ligands of the cubane cluster, thus exerting a direct conjugation to each of the four cobalt sites. To this aim the isostructural series with formula $[Co^{III}_4(\mu\text{-}O)_4(\mu\text{-}CH_3COO)_4(p\text{-}NC_5H_4X)_4]$, hereafter **1-X** (X = Me, *t*-Bu, OMe, Br, COOMe, CN, Scheme 1b) has been screened for WOC under dark and illumination conditions. The impact of ligand substitution has been evaluated on (i) the electrocatalytic properties of the cobalt cubane, (ii) the rate of primary photoinduced ET events (Scheme 1a), and (iii) the photosynthetic performance for O_2 production. An unprecedented structure−reactivity analysis emerges herein, highlighting the importance of ET tuning within a photosynthetic sensitizer/catalyst system by stereoelectronic ligand modification.

The isostructural complexes are obtained according to literature protocols,[20] and their solution identity and stability has been confirmed by NMR and ESI-MS (see SI). Inspection of the **1-X** WOC properties has been initially addressed under dark conditions, with cyclic voltammetry (CV), by evaluating the water discharge overpotentials (η) and the onset of a catalytic current.[26] These experiments confirm that **1-X** can actually perform water oxidation, with overpotentials varying in a narrow range (0.50−0.57 V, Table 1 and Figure S2), but with no apparent ordering effect as a function of the pyridine substituent. The impact of ligand substitution has been then explored under irradiation conditions, within the sacrificial $Ru(bpy)_3^{2+}/S_2O_8^{2-}$cycle. In this system, photocatalytic turnovers are triggered by sequential "hole scavenging" events, involving consecutive ET steps from the cobalt cubane to photogenerated $Ru(bpy)_3^{3+}$.[27]

Table 1. Water Oxidation by 1-X Isostructural Catalysts

X[a]	η (V)[b]	k (10^8 M^{-1} s^{-1})[c]	$E_{1/2}$ (mV)[d]	QE (%)[e]
OMe	0.57	2.51	877	80[f]
Me	0.52	1.92	880	30
t-Bu	0.50	1.39	855	10
H	0.55	1.33	926	26
Br	0.53	0.60	990	32
COOMe	0.51	0.70	1040[g]	46
CN	0.51	0.14	1081[g]	26

[a]Substituent in *para*-position on the pyridine ligand, see Scheme 1b. [b]Overpotential of water discharge in 0.2 M aqueous phosphate buffer (pH 7), determined at an anodic current value of 50 μA (current density = 0.7 mA·cm^{-2}) with a scan rate = 100 mV/s. [c]Bimolecular rate constant for ET in eq 1 in 50:50 acetonitrile:10 mM aqueous borate buffer (pH 8). [d]$E_{1/2}$(**1-X**$^+$/**1-X**) in 50:50 CH_3CN/10 mM aqueous borate buffer (pH 8), vs Ag/AgCl. [e]Quantum efficiency obtained for the photochemically driven process (λ_{exc} = 450 nm), determined over the first 30 min of reaction (see note 25). [f]Maximum value observed with freshly prepared solutions of **1-OMe**, see text. [g]$E_{1/2}$ in 50:50 CH_3CN/10 mM aqueous phosphate buffer (pH 7) since the waves in 50:50 CH_3CN:10 mM aqueous borate buffer (pH 8) are not resolved due to overlapping with water oxidation discharge (see Figures S4 and S5).

The primary ET rate (eq 1) is accessible through flash photolysis technique. In these experiments, a given concen-

$$\textbf{1-X} + Ru(bpy)_3^{3+} \rightarrow \textbf{1-X}^+ + Ru(bpy)_3^{2+} \quad (1)$$

tration of oxidized sensitizer is generated "instantaneously" (i.e., within 10 ns) by photoreaction of the pristine $Ru(bpy)_3^{2+}$ with the $S_2O_8^{2-}$sacrificial acceptor, and its reaction with the catalyst is monitored over a relatively wide time window (0−100 ms). These experiments show that $Ru(bpy)_3^{3+}$ (detected by the bleach at 450 nm) is reduced back to $Ru(bpy)_3^{2+}$ with kinetics dependent on the catalyst concentration as monitored by the absorbance increase at 450 nm. The bimolecular rate constant for the ET process can be then obtained, assuming pseudo-first-order kinetic conditions, by linear plots of rate constants vs catalyst concentration (Figure 1a).

For **1-H** in buffered water, primary ET was previously found to have a bimolecular rate constant, $k = (1.2-1.6) \times 10^7$ M^{-1} s^{-1}.[21a] Under those conditions, however, the recovery of $Ru(bpy)_3^{2+}$ never reached completion in the flash photolysis experiments. This was mainly ascribed to a low thermodynamic

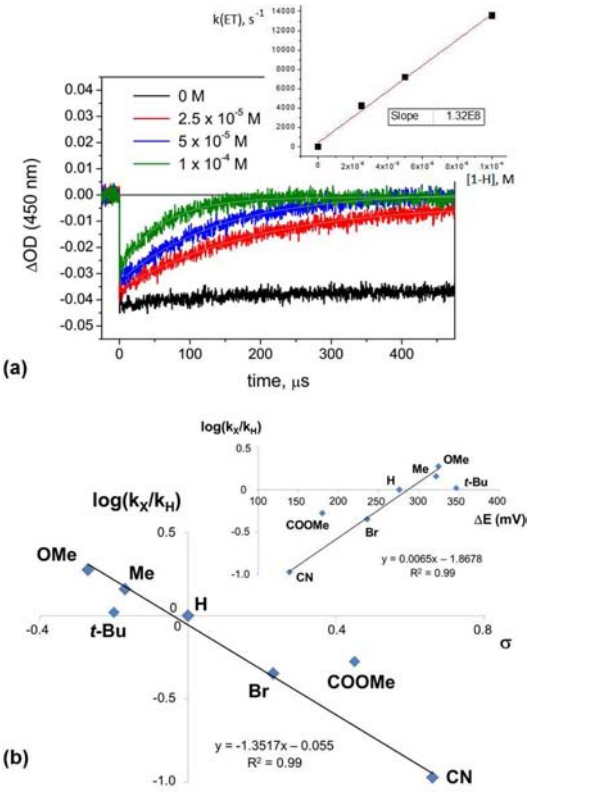

Figure 1. (a) Flash photolysis experiments (λ_{exc} = 355 nm) in 50:50 acetonitrile:10 mM aqueous borate buffer (pH 8) containing 50 μM $Ru(bpy)_3^{2+}$, 0−100 μM **1-H**, and 5 mM $S_2O_8^{2-}$. Inset: linear fit of kinetic rate constants vs [**1-H**] plot for obtaining the bimolecular rate constant. (b) Hammett linear free energy relationship plot of photoinduced ET rate constants (see text and Table 1). Inset: plot of photoinduced ET rate constants vs redox potential gap Δ= $E(Ru(bpy)_3^{3/2+})$ − E(**1-X**$^+$/**1-X**).

dx.doi.org/10.1021/ja303951z | J. Am. Chem. Soc. 2012, 134, 11104−11107

driving force dictating the ET process in buffered water, where the redox couples $Ru(bpy)_3^{3+}/Ru(bpy)_3^{2+}$ and **1-H**$^+$/**1-H** exhibit similar potentials (1.06 and 1.05 V, respectively, vs Ag/AgCl, NaCl 3 M).[21] The acceptor−donor redox gap can be remarkably enhanced in 50:50 CH_3CN/10 mM aqueous borate buffer (pH 8), where the experimental potentials turn out to be 1.202 and 0.926 V, respectively (Figure S5). The mixed solvent not only guarantees the proper thermodynamic boost for quantitative ET and complete recovery of the $Ru(bpy)_3^{2+}$ absorption, but also brings about a strong acceleration of the ET rate, with $k_H = 1.33 \times 10^8$ M^{-1} s^{-1}, that is 1 order of magnitude higher than in buffered water[21a] (Table 1 and Figure 1). This is a key observation, as the time domain of photoinduced ET within the photosynthetic assembly is pivotal for the both required multihole accumulation upon sequential ET and the sensitizer stability. This latter is a major requirement for durability of artificial systems applied to water splitting for a viable hydrogen economy.

In the mixed solvent, complete recovery of the $Ru(bpy)_3^{2+}$ absorption is obtained with all the isostructural **1-X** complexes. Moreover, a remarkable ligand effect is observed on the ET kinetics as a function of the pyridine substituent, with k_X in the range $(0.14-2.51) \times 10^8$ M^{-1} s^{-1} (Table 1 and Figure 1). A Hammett linear free energy relationship (LFER) is obtained by plotting $\log(k_X/k_H)$ versus the substituent σ constants. The Hammett analysis provides a negative slope value, $\rho = -1.3$, indicating that photoinduced ET is favored by electron-rich pyridine ligands (Figure 1b).[28] While a similar approach has been previously reported in light-activated porphyrin dyads,[29] this evidence is unprecedented for photosynthetic assemblies involving multimetal cores.

The direct participation of the cobalt core is also confirmed by the parallel analysis of the **1-X**$^+$/**1-X** redox potentials in CH_3CN/buffered water media (Table 1 and Figures S4, S5, S9−S15). Indeed, the $\log(k_X/k_H)$ values correlate with the redox potential gap $\Delta E = \{E_{1/2}(Ru(bpy)_3^{3+/2+}) - E_{1/2}(\mathbf{1\text{-}X}^{+/0})\}$, see inset in Figure 1b. This observation confirms that photoinduced ET rate increases with increasing the sensitizer/catalyst ΔE, and then it occurs in the Marcus normal region of classical ET theory being accelerated by a higher thermodynamic driving force.[28]

While time-resolved spectroscopy dissects the first event of the photocatalytic cycle (eq 1), the overall performance of the system is probed by evaluating (i) the oxygen production yield, (ii) the catalytic turnover number (TON), and (iii) the QE. To this aim, the oxygenic activity of the **1-X** series has been investigated in the presence of an excess of the $Ru(bpy)_3^{2+}/S_2O_8^{2-}$ couple. In a typical experiment, irradiation with an halogen lamp at $\lambda > 400$ nm of **1-X** (18 μM) in 50:50 acetonitrile:10 mM aqueous borate buffer (pH 8) containing 1 mM $Ru(bpy)_3^{2+}$ and 5 mM $S_2O_8^{2-}$ leads to continuous oxygen production with the time evolution profiles reported in Figure 2. Under the conditions explored, the kinetics obey to a zero-order law, up to >80% of persulfate consumption, likely depending on the applied photon flux, which maintains a stationary state of photogenerated $Ru(bpy)_3^{3+}$.

At variance with what was observed in aqueous buffer,[21] in the mixed solvent, oxygen evolution occurs until quantitative consumption of the sacrificial electron acceptor (solid line in Figure 2), corresponding to a total of 140 turnovers (TON = (mol O_2)/(mol cat.)) for all **1-X** catalysts (Figures 2 and S17). Such major improvement of the photosynthetic performance

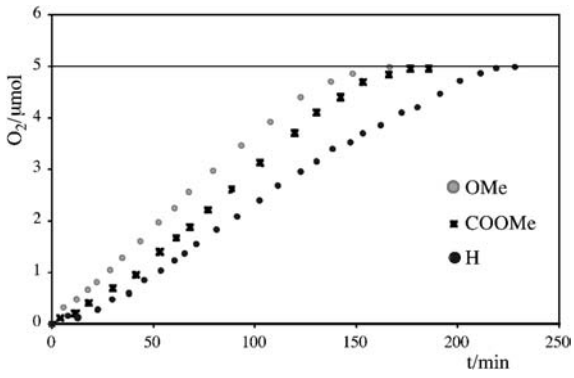

Figure 2. Oxygen production kinetics by [**1-X**] = 18 μM (X = H, COOMe, OMe as representative substrates), $[Ru(bpy)_3^{2+}]$ = 1 mM, $[S_2O_8^{2-}]$ = 5 mM in 2 mL of 50:50 acetonitrile:10 mM borate buffer (pH 8), $\lambda_{irr} > 400$ nm, with a 50 W halogen lamp; see SI.

can result from an improved stability of the $Ru(bpy)_3^{2+}$ photosensitizer, as confirmed by UV−vis spectra (Figure S16).

The most relevant descriptor addressing performance in photoinduced processes is, without doubt, the resulting QE.[25,30] The QE values for the **1-X** catalysts, determined from the oxygen evolution rate over the first 30 min, are reported in Table 1. In particular, a record value of 80% has been observed for **1-OMe**, setting a new benchmark in photoactivated water oxidation catalysis.

At variance with the primary ET process, the QE trend is not showing a straightforward dependence on the ligand electronic effect. The observed QE order turns out as follows: OMe > COOMe > Me ≈ H ≈ Br ≈ CN > *t*-Bu (Table 1). This result is probably related to an overall balance of competing factors crowning over diverse steps before oxygen release, and likely involving a multifaceted $Co^{III/IV}$ manifold. In particular, water coordination equilibria and the nucleophilic attack to metal-oxo intermediates, for O−O bond formation, are expected to be favored by electron-withdrawing ligands. The final scenario is nevertheless converging on the supremacy of the **1-OMe** term, bringing about the fastest ET and the exceptional QE of 80% determined for oxygen evolution under visible light irradiation (λ = 450 nm).

After the work by Finke et al., the question on the molecular nature of the competent WOC calls for attention.[31] In the case of **1-X**, the strong impact observed upon subtle substituent changes in the periphery of the pyridine ligands is indicative of a molecular mechanism.[31]

In summary, structure−reactivity correlations spanning throughout the dissection of mechanistic events provide a key guide to direct our quest for innovative molecular WOCs and cost-effective artificial photosynthetic devices.

■ ASSOCIATED CONTENT

Ⓢ Supporting Information

Synthesis, characterization, electrochemistry, flash photolysis studies, and kinetics. This material is available free of charge via the Internet at http://pubs.acs.org.

■ AUTHOR INFORMATION

Corresponding Author

andrea.sartorel@unipd.it; snf@unife.it; campagna@unime.it; marcella.bonchio@unipd.it

Notes

The authors declare no competing financial interest.

■ ACKNOWLEDGMENTS

We thank Valerio Doppio (University of Padova) for preliminary experiments. Financial support from MIUR (FIRB Nanosolar RBAP11C58Y), University of Padova (PRAT 2010 CPDA104105/10, 2008 HELIOS project STPD08RCX), and Fondazione Cariparo (Nanomode Progetti di Eccellenza 2010) is gratefully acknowledged.

■ REFERENCES

(1) Gust, D.; Moore, T. A.; Moore, A. L. *Acc. Chem. Res.* **2009**, *42*, 1890.
(2) Gray, H. B. *Nat. Chem.* **2009**, *1*, 7.
(3) Lewis, N. S.; Nocera, D. G. *Proc. Natl. Acad. Sci. U.S.A.* **2006**, *103*, 15729.
(4) Meyer, T. J. *Nature* **2008**, *451*, 778.
(5) Sartorel, A.; Carraro, M.; Toma, F. M.; Prato, M.; Bonchio, M. *Energy Environ. Sci.* **2012**, *5*, 5592.
(6) Youngblood, W. J.; Lee, S.-H. A.; Kobayashi, Y.; Hernandez Pagan, E. A.; Hoertz, P. G.; Moore, T. A.; Moore, A. L.; Gustand, D.; Mallouk, T. E. *J. Am. Chem. Soc.* **2009**, *131*, 926.
(7) La Ganga, G.; Nastasi, F.; Campagna, S.; Puntoriero, F. *Dalton Trans.* **2009**, 9997.
(8) Zhang, J.; Grzelczak, M.; Hou, Y.; Maeda, K.; Domen, K.; Fu, X.; Antonietti, M.; Wang, X. *Chem. Sci.* **2012**, *3*, 443.
(9) Najafpour, M. M.; Ehrenberg, T.; Wiechen, M.; Kurz, P. *Angew. Chem., Int. Ed.* **2010**, *49*, 2233.
(10) Jiao, F.; Frei, H. *Energy Environ. Sci.* **2010**, *3*, 1018.
(11) Hocking, R. K.; Brimblecombe, R.; Chang, L.-Y.; Singh, A.; Cheah, M. H.; Glover, C.; Casey, W. H.; Spiccia, L. *Nat. Chem.* **2011**, *3*, 461.
(12) Kanan, M. W.; Nocera, D. G. *Science* **2008**, *321*, 1072.
(13) Gerken, J. B.; McAlpin, J. G.; Chen, J. Y. C.; Rigsby, M. L.; Casey, W. H.; Britt, R. D.; Stahl, S. S. *J. Am. Chem. Soc.* **2011**, *133*, 14431.
(14) Herrero, C.; Quaranta, A.; Leibl, W.; Rutherford, A. W.; Aukauloo, A. *Energy Environ. Sci.* **2011**, *4*, 2353.
(15) Duan, L.; Tong, L.; Xu, Y.; Sun, L. *Energy Environ. Sci.* **2011**, *4*, 3296.
(16) Huang, Z.; Luo, Z.; Geletii, Y. V.; Vickers, J. W.; Yin, Q.; Wu, D.; Hou, Y.; Ding, Y.; Song, J.; Musaev, D. G.; Hill, C. L.; Lian, T. *J. Am. Chem. Soc.* **2011**, *133*, 2068.
(17) Puntoriero, F.; La Ganga, G.; Sartorel, A.; Carraro, M.; Scorrano, G.; Bonchio, M.; Campagna, S. *Chem. Commun.* **2010**, *46*, 4725.
(18) Karlsson, E. A.; Lee, B. L.; Åkemark, T.; Johnston, E. V.; Karkas, M. D.; Sun, J. L.; Hansson, O.; Backvall, J. E.; Åkemark, B. *Angew. Chem., Int. Ed.* **2011**, *50*, 11715.
(19) Concepcion, J. J.; Jurss, J. W.; Brennaman, M. K.; Hoertz, P. G.; Patrocinio, A. O. T.; Murakami Iha, N. Y.; Templeton, J. L.; Meyer, T. J. *Acc. Chem. Res.* **2009**, *42*, 1954.
(20) Chakrabarty, R.; Bora, S. J.; Das, B. K. *Inorg. Chem.* **2007**, *46*, 9450.
(21) (a) La Ganga, G.; Puntoriero, F.; Campagna, S.; Bazzan, I.; Berardi, S.; Bonchio, M.; Sartorel, A.; Natali, M.; Scandola, F. *Faraday Discuss.* **2012**, *155*, 177. (b) McCool, N. S.; Robinson, D. M.; Sheats, J. E.; Dismukes, G. C. *J. Am. Chem. Soc.* **2011**, *133*, 11446.
(22) Steinmiller, E. M. P.; Choi, K.-S. *Proc. Natl. Acad. Sci. U.S.A.* **2009**, *106*, 20633.
(23) Zhong, D. K.; Gamelin, D. R. *J. Am. Chem. Soc.* **2010**, *132*, 4202.
(24) Reece, S. Y.; Hamel, J. A.; Sung, K.; Jarvi, T. D.; Esswein, A. J.; Pijpers, J. J. H.; Nocera, D. G. *Science* **2011**, *334*, 645.
(25) QE is the normalized quantum yield (QY), defined as QE = $(QY/QY_{MAX}) \times 100$, where QY_{MAX} is the theoretical maximum value, derived from the operating photosynthetic scheme. QE is a useful parameter to compare the performance of photosynthetic systems, regardless of the reaction scheme leading from absorbed photons to products.
(26) Analysis of the normalized CVs ($i/\nu^{1/2}$) has been performed for **1-COOMe**, as representative case, at different scan rates (ν = 25−1600 mV/s, Figure S3). The peak current (1.3 V vs Ag/AgCl) normalized to the square root of the scan rate increases with decreasing the scan rate, which is generally associated with a rate-limiting chemical step followed by fast ET within an electrocatalytic cycle. Chen, Z.; Concepcion, J. J.; Luo, H.; Hull, J. F.; Paul, A.; Meyer, T. J. *J. Am. Chem. Soc.* **2010**, *132*, 17670.
(27) Puntoriero, F.; Sartorel, A.; Orlandi, M.; La Ganga, G.; Serroni, S.; Bonchio, M.; Scandola, F.; Campagna, S. *Coord. Chem. Rev.* **2011**, *255*, 2594.
(28) Photoinduced ET rates appear to be mainly controlled by the thermodynamic driving force, as a well-behaved linear Hammett correlation is obtained with the experimental redox potentials of **1-X** (Figure S6). However, other stereoelectronic factors come into play, likely determined by sensitizer/catalyst supramolecular interactions. While the negative deviation of **1-*t*-Bu** in the LFER plot of Figure 1 can easily be assigned to steric hindrance, the positive deviation of **1-COOMe** compensating for the thermodynamic fall is under investigation.
(29) Gust, D.; Moore, T. A.; Moore, A. L.; Kang, H. K.; DeGraziano, J. M.; Liddell, P. A.; Seely, G. R. *J. Phys. Chem.* **1993**, *97*, 13637.
(30) TOF values for the **1-X** series fall in the range $(7.1-1.3) \times 10^{-2}$ s^{-1}, with a photon flux of 2×10^{-9} einstein s^{-1} at λ = 450 nm. TOFs are frequently used to evaluate the efficiency of photo-driven catalytic processes. However, these are highly dependent on the applied photon flux. For such reasons, any comparison among photo-driven TOFs with diverse irradiation, or with respect to dark catalysis values, is misleading. As remarked, QE provides the most relevant parameter to evaluate the photosynthetic performance; see also: Natali, M.; Orlandi, M.; Berardi, S.; Campagna, S.; Bonchio, M.; Sartorel, A.; Scandola, F. *Inorg. Chem.* **2012**, DOI: 10.1021/ic300703f.
(31) Stracke, J. J.; Finke, R. G. *J. Am. Chem. Soc.* **2011**, *133*, 14872. Prolonged aging (24 h) of **1-OMe** in the reaction mixture causes a modification of the UV/vis spectrum, a minor broadening of the ^{1}H NMR signals (Figures S7 and S8), and a parallel reduction of QE by up to 30%, indicating that a possible leaching of paramagnetic Co(II) ions leads to a drop of the catalytic activity.